Research on Engineering Structures & Materials
www.jresm.org
Research Group

Research Article

Seismic response prediction using a hybrid unsupervised and supervised machine learning in case of 3D RC frame buildings

Benbokhari Abdellatif[1,a*], Benazouz Chikh[1,b] , Mébarki Ahmed[2,3,c]

[1]*Laboratoire des Travaux publics, ingénierie de Transport, environnement, Ecole Nationale Supérieure des Travaux Publics, Algeria*
[2]*UPEC, CNRS, Laboratory Modélisation et Simulation Multi Echelle, University Gustave Eiffel, France*
[3]*Nanjing Tech University, China*

Article Info

Article history:

Received 29 Dec 2023
Accepted 20 Mar 2024

Keywords:

Nonlinear dynamic analysis;
Machine learning;
Seismic response prediction;
Unsupervised algorithms;
Artificial neural networks

Abstract

The seismic vulnerability assessment represents an important step in monitoring the buildings' capacity and checking their performance during and after earthquake events. The Nonlinear Time History Analysis (NL-THA) is considered the most reliable method that is used to calculate the exact structural behavior of any building. However, this sophisticated method is known for its complexity, the use of Finite Element (FE) software, and computational time consuming, especially in the case of tall buildings. For that reason, An Artificial Neural network (ANN) is used to develop a new model able to predict the essential Engineering Demand Parameters (EDPs), i.e., the Maximum Base Shear (MBS), the Maximum Inter-story Drift (MIDR) and the Maximum Roof Drift Ratio (RDR). Unsupervised algorithms such as the Principal Component Analysis PCA and the Autoencoder are coupled with the ANN to reduce the dimensionality, improve the dataset quality, and reduce the irrelevant features. More than 192,000 buildings are analyzed using the NL-THA and eighty artificial ground motions (GMs) to generate the dataset. The buildings' characteristics are generated randomly from the selection range. The results showed that the Autoencoder-ANN model represents the highest performance compared to the PCA-ANN and ANN models. The Autoencoder-ANN model could quickly and accurately predict the seismic responses of unseen ground motions using only the building's characteristics and the GM parameters without using any FE software.

1. Introduction

Earthquakes are unpredictable phenomena that may occur anywhere and anytime. Their energy is released as seismic vibrations affecting the buildings and infrastructure, which can be devastating [1]. Several earthquakes have been recorded in the last decade, resulting in enormous human losses and severe damage to infrastructure and strategic buildings [2]. Therefore, the preparedness and seismic vulnerability assessment is mandatory to protect lives, reduce economic losses, and maintain the functionality of essential structures like bridges, hospitals, and emergency offices [3-4].

Many researchers developed methodologies and approaches to study and estimate structures' seismic vulnerability and fragility [5-11]. The most reliable and accurate approach is the Nonlinear Time History Analysis (NL-THA) [12]. This approach is based on solving a complicated differential equation of motion. The results of the NL-THA can be used to construct fragility curves by performing Incremental Dynamic Analysis (IDA) and probabilistic calculations. These curves represent the probability of exceeding a specific

*Corresponding author: a.benbokhari@enstp.edu.dz
[a]orcid.org/0000-0002-0819-0641; [b]orcid.org/0000-0002-7228-9224; [c]orcid.org/0000-0002-3361-2594
DOI: http://dx.doi.org/10.17515/resm2024.137me1229rs

Intensity Measure (IM) damage level. This process can be used to estimate the cost needed to rehabilitate buildings in case of an earthquake event. However, the NL-THA and the IDA are considered time-consuming approaches that require suitable hardware and expertise, making the assessment process complex and take a long time [13-14].

Many numerical, mechanical, and empirical approaches are proposed to estimate the seismic response and assess buildings' seismic vulnerability and fragility [15-18]. Nevertheless, these approaches may represent some substantial uncertainties and less accuracy than the NL-THA results. Several new techniques have been proposed, including using artificial intelligence and Machine Learning (ML) in this field. These techniques showed promising results and potential in terms of predictability and high accuracy of the seismic response and damageability assessment of structures [19-21].

Vafaei et al. [22] used the ANN to detect the seismic damage of concrete shear walls, and they found that the ANN model successfully predicted the damages induced by an earthquake. Morfidis et al. [23] proposed a rapid seismic damage prediction of RC buildings methodology using the ANN. They used 30 RC buildings and 65 ground motions to train the ANN model, and it was found that the ANN can predict the damage indices precisely for seen GMs and with acceptable results in the case of unseen buildings and GMs. Oh et al.[24] proposed an ANN-based seismic response prediction using artificial 2700 GMs, where they proposed a new parameter related to the frequency domain and the resonance area. The model was validated using a 2D Multi degrees of freedom structure, and the method showed high accuracy in predicting the MIDR. In addition, Won et al. [25] developed a machine-learning approach for predicting the seismic damage of an equivalent Single degree of freedom considering the soil-structure interaction. The results of their paper were that the ANN model managed to accurately predict the damage level using only the idealized bilinear capacity curve parameters, soil, and earthquake characteristics. Furthermore, Petros and Vitor [26] used the ANN to model the seismic vulnerability of building portfolios, where they found a remarkable prediction of the structural response, economic loss, and damage level. They mentioned in their work that the ANN was an accurate technique to be used as a probabilistic seismic risk assessment method. Seo et al. [27] and Hait et al. [28] use the ML models to assess the seismic vulnerability of irregular structures and derive fragility curves quicker.

Finally, Machine learning use was not only applied to buildings but on some infrastructures such as bridges [29-31].

Based on the literature review, The proposed ML models show a valuable and promising method for seismic response prediction as accurate as the NL-THA results. However, it is essential to note that the studies mentioned in the literature review have some limitations. They are based on a small range of building characteristics and lack generalization. Furthermore, in some of these works, their generalized models could have achieved higher accuracy. Additionally, in some other cases, the prediction process needs software modeling to calculate input characteristics like the center of torsion and the period vibration of the fundamental mode. Furthermore, this paper compared the performance of three ML models to investigate the impact of the use of unsupervised algorithms on the ML performance.

This paper presents a ML model that can predict three Engineering Demand Parameters (EDPs) using only the geometric and loading characteristics of structures with the artificial ground motions (AGMs) parameters, without the need for additional Finite Element (FE) calculations. The EDPs in question are the Maximum Base Shear (MBS), the Maximum Inter-story Drift (MIDR), and the Maximum Roof Drift Ratio (RDR). These parameters are crucial in designing structures, as they help engineers estimate the MBS and control the structure's performance using the MIDR and MRDR.

The proposed method generates a dataset using OpenSees and performs over 192,000 Non-Linear Time-History Analyses (NL-THA). The characteristics of the buildings are selected randomly from a range of options, including the Number of Stories (Ns), Number of Bays in x-x direction (Nbx), Number of Bays in y-y direction (Nby), Story Height (Hs), Bays' Length in x-x direction (Lbx), Bays' Length in y-y direction (Lby), Column Dimensions (b,h), Beam Dimensions (b1,h1), Reinforcement Area of Column (As_col), Reinforcement Area of Beams (As_beam), Compression Strength of Concrete (fc28), Yielding Limit Stress of Rebars (fy), Permanent Surface Load (G), and Live Surface Load (Q). To perform the NL-THA and generate the dataset, the method generates eighty artificial and synthetic GMs and matches them to the target response spectrum (EuroCode-8).

Three ANN models are used to establish the relationship between the inputs and outputs. The first model uses the original dataset as input data. In the second model, a Principal Component Analysis (PCA) is applied to the input data to identify the principal components, which are then used as inputs. The third model utilizes an Autoencoder technique to capture the essential features of the dataset and reduce its dimensionality. To evaluate the models' predictability, 80 AGMs are generated and matched to the same target response spectrum. These AGMs are then used to perform a NL-THA on three case study buildings. Finally, the accuracy of the models in fragility assessment is determined by generating 3D fragility surfaces using the NL-THA and the three ANN models.

2. Methodology

This work aims to develop an ANN model to predict the maximum seismic response of a 3D RC frame building subjected to unseen GMs. In order to reach the objective, the first step is to create the dataset with OpenSees. The 3D model will be subjected to eighty AGMs, and NL-THA will be performed to calculate the MBS, MIDR, and MRDR. Figure 1 shows that the methodology is based on three main steps, which are explained in detail in the following sections.

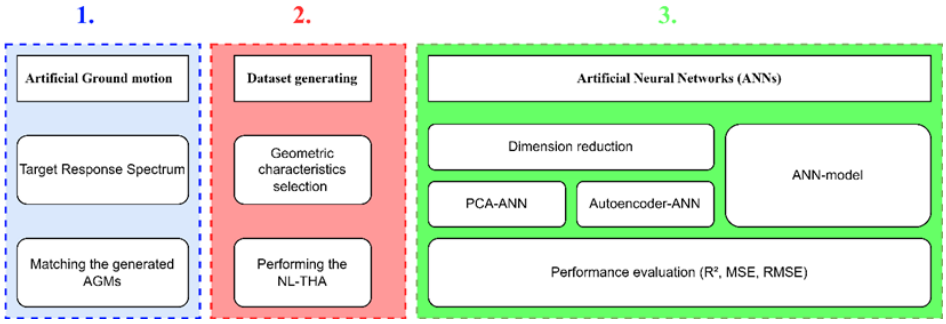

Fig. 1. The flowchart of the used methodology

2.1. Ground motion selection

The ground motion selection represents an essential step in performing a fragility assessment, mainly when we aim to construct fragility curves [32] [33]. Choosing the proper seismic record is challenging for analysts, especially when dealing with actual ground motion records [34]. In some cases, the studied area does not have the required ground motion records. In addition, real GMs may have a long duration, and that will affect the NL-THA calculation time. Therefore, using a generated ground motion is the best alternative to solve these problems. Artificial and synthetic ground motions are different algorithms used to generate unreal ground motion that satisfies some conditions. The user

can fix the earthquake parameters for synthetic accelerograms, e.g.: near/ far -field, moment magnitude, and soil parameters [35]. Only the shape envelope and the accelerogram duration are needed for the artificial GMs to generate a GM. For this study, eighty AGMs have been generated and matched to an EC8 target response spectrum. The target spectrum is generated using the EC8, considering the following parameters:

- Ground acceleration (A_g): 0.2 (g)
- Spectrum type: Type I.
- Importance class: II.

Figure 2 illustrates the mean-matched response spectra, the generated GMs, and the target response spectrum. Table A.1 represents the earthquake parameters of the generated GMs. Twenty-one parameters in Table 1 characterize the ground motions used in the ANN.

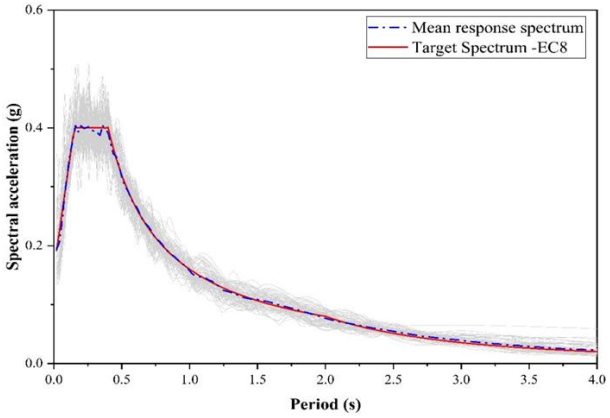

Fig. 2. The generated ground motions and their mean response spectrum and the target spectrum

Table 1. The ground motion characteristics

	Definition	Equation
PGA	Peak ground acceleration	= Max |acceleration(t)|
PGV	Peak ground velocity	= Max |velocity(t)|
PGD	Peak ground displacement	= Max |displacement(t)|
E_{cum}	Cumulative energy	$= \int_0^{t=end} acceleration(t)^2.dt$
I_a	Arias intensity	$= \frac{\pi}{2g}\int_0^{Td} acceleration(t)^2 dt$
CAV	Cumulative Absolute velocity	$= \int_0^{Tmax} \|a(t)\|dt$
Sa	Spectral acceleration (T1)	$= (\frac{2\pi}{T1})^2 \times Sd\ (T1)$
Sv	Spectral velocity (T1)	$= (\frac{2\pi}{T1}) \times Sd\ (T1)$
Sd	Spectral displacement (T1)	$=\frac{1}{m\times\omega}\max\left(\left\|\int_0^t p(\tau)\, e^{-\zeta\omega_n(t-\tau)} \sin[\omega_D\,(t-\tau)]\, d\tau\right|\right)$
U_T	Uniform duration	The cumulative duration of exceeding 5% of PGA

B_T	Bracket duration	The total duration between the first and the last exceedance of a 5% of PGA.
HI	Housner intensity	$= \int_{0.1}^{2.5} PSV\ (\zeta = 5\%, T) dT$
PP	predominant period	The period corresponding to the maximum Sa ($\zeta = 5\%$)
SD	Significant duration	The duration interval between 5% and 95% of the cumulative intensity arias
ASI	Acceleration Spectrum Intensity	$= \int_{0.1}^{0.5} Sa\ (\zeta = 5\%, T)\ dT$
VSI	Velocity Spectrum Intensity	$= \int_{0.1}^{0.5} Sv\ (\zeta = 5\%, T)\ dT$
DSI	Displacement Spectrum Intensity	$= \int_{0.1}^{0.5} Sd\ (\zeta = 5\%, T)\ dT$
SI	Response spectrum intensity	$= \int_{0.1}^{2.5} Sv\ (\zeta = 5\%, T)\ dT$
D_f	Dominant frequency	The frequency that carries out the highest amount of energy
B_w	Bandwidth	The difference between the lower and upper frequencies of a certain thresholds (-3db)
f_c	central frequency	The mean frequency between the upper and the lower frequencies.

2.2. Dataset Generation with The Nonlinear Time-History Analysis

NLTHA is a type of dynamic structural analysis used to simulate complex multiple support excitations at certain points on the structure. It is one of the most reliable methods used to calculate the exact structural behavior of any building during an earthquake event. It is based on solving a complicated differential equation of motion, and its results can be used to construct fragility curves by performing the Incremental Dynamic Analysis (IDA) and probabilistic calculations. However, the NL-THA is known for its complexity, the use of Finite Element (FE) software, and computational time-consuming, especially in the case of tall buildings. The outputs of this analysis can be an engineering demand parameter (EDPs) such as IDR, RDR or story displacement in a form of time series. OpenSees can be used to perform this analysis and to generate the dataset needed for this study.

The followed process of generating the dataset using OpenSees is illustrated in Figure 3 and explained below:

- Start by creating a model in OpenSees. For a time, history analysis, this would include defining nodes and elements, assigning boundary conditions, specifying material properties and assembling the system into a model.
- Create the ground motion records that represent earthquake loading on your structure then format and transform them such that they can be used in OpenSees as prescribed loading. a scale factor should be specified in this step to scale the ground motion, and their characteristics should be calculated and recorded (PGA, PGV, PGD, Ecum, Ia, CAV…etc.)
- Specify the type of analysis, the solution algorithm (e.g.: KrylovNewton, SecantNewton , ModifiedNewton , RaphsonNewton) , the integrator , and the the convergence test (e.g.; NormDispIncr, RelativeEnergyIncr, EnergyIncr, RelativeNormUnbalance.

Run the simulation in OpenSees after specifying the control node, direction, number of degrees of freedom and the needed responses (e.g., acceleration, velocity, displacement, reactions, drift).

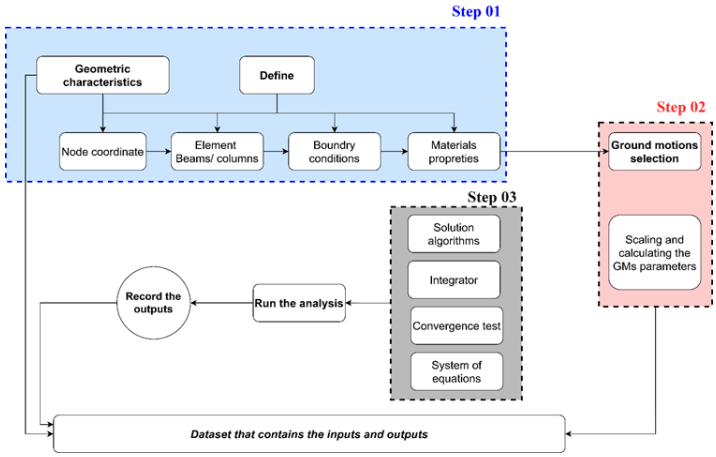

Fig. 3. The followed process on OpenSees to perform the NLTHA

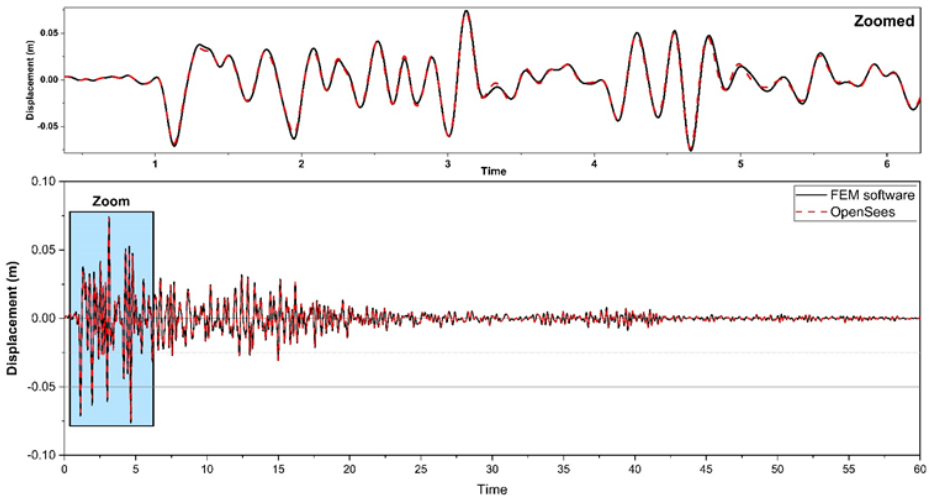

Fig. 4. The displacement history of a 4-story RC frame subjected to El-Centro GM scaled to PGA = 0.4g

Figure 4 illustrates the displacement time history of a 4-story RC frame building subjected to El-Centro ground motion scaled to PGA = 0.4 g using FEM software and OpenSees. It shows that the OpenSees model accurately estimates and find the displacement response of the validation model.

The dataset is generated using OpenSees by performing the NL-THA. The buildings are created by randomly selecting their geometric and material characteristics from the selection range, as shown in Table 2. The geometric and material characteristics are illustrated in Figure 5. In this work, it is considered that we have two types of loads (permanent load (G) and live load (Q)). The yielding and the ultimate strain of the concrete are -0.2% and -0.35%, and "concrete02" is used in OpenSees. A 200 GPa is the young modulus of the reinforcement steel with a zero-post yielding ratio, and the "Steel02" is used in OpenSees.

Table 2. The structural characteristics and the selection range (min, max and step)

Parameter	Unit	Min	Step	Max
Ns	-	1	1	10
Hs	m	3	0.2	4
Nbx	-	1	1	6
Lbx	m	3.5	0.5	6
Nby	-	1	1	6
Lby	m	3.5	0.5	6
h	cm	25	0.05	100
b	cm	25	0.05	100
h1	cm	25	0.05	50
b1	cm	25	0.05	50
As_col	cm^2	9.0432	0.2512	64.3072
As_beam	cm^2	9.0432	0.2512	64.3072
G	kN/m^2	1	1	6
Q	kN/m^2	1	1	6
fc28	MPa	25	5	45
fy	GPa	350	50	550

After selecting the required geometric and material characteristics and selecting the GM, and scaling it, an NL-THA is performed, and the seismic response is captured, i.e., MBS, MISDR, and MRDR. These characteristics and the seismic response represent the input and the outputs that will be used in the machine-learning algorithms. As a result, a dataset has been generated that contains 192,092 NL-THA using eighty artificial and synthetic GMs, and this dataset should be preprocessed before using it in the ML.

Figure 6 displays a heatmap which shows the correlation between the various features of the dataset, including inputs and outputs. Upon examining the heatmap, it becomes apparent that there is a strong positive correlation between the MIDR and the ground motion parameters such as PGA, PGV, Ecum, Ai, CAV, Sa, Sv, HI, ASI, VSI, DSI, and SI. Conversely, there is a negative correlation between the MIDR and structural geometry parameters such as h, b, N_{bx}, N_{by}, and b_1. The MRDR exhibits the same correlation with the GMs parameters and structural geometry as the MIDR. This correlation helps to identify the most critical features that impact the performance or damage incurred during an earthquake event. For the MBS, It is affected positively with the earthquake parameters (PGA, PGV, Ecum, AI, ASI, VSI, DSI, SI) and negatively with the structural geometry (Nbx, Nby and As_column).

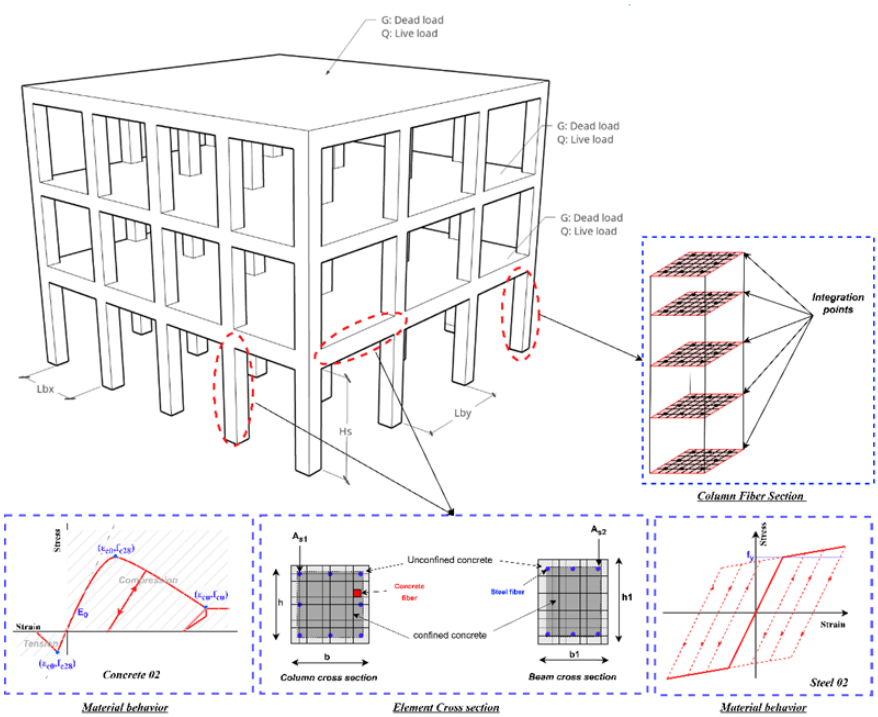

Fig. 5. The geometric characteristics of the 3D RC frame building

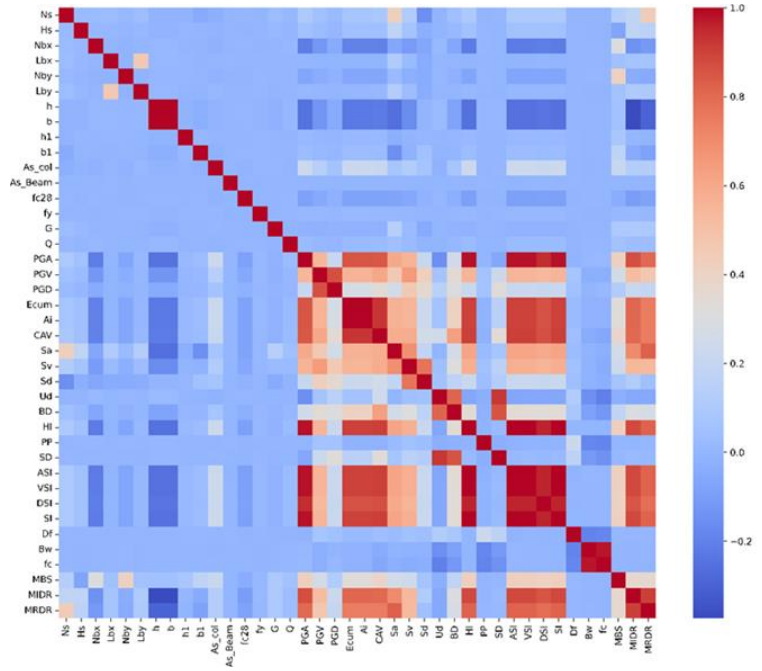

Fig. 6. The degree of correlation between the generated dataset features (inputs and outputs)

2.3. Principal Component Analysis (PCA)

The PCA is one of the most used techniques for dimensionality reduction. It is an unsupervised machine learning algorithm that aims to capture the principal components of the dataset. The data reorientation allows us to use fewer dimensions without losing much information. In addition, this technique may reduce the data noises and the irrelevant features that can affect the training time, the performance, and the hyperparameters optimization of the ANN. The PCA is based on transforming the correlated variables into uncorrelated new variables using a linear combination. The eigenvalues and the cumulative variability of each principal component are illustrated in Figure 7. If 90% of the variability is fixed as a threshold, twenty principal components will be used as inputs of the ANN model.

2.4. Autoencoder Algorithm

The autoencoder is a type of ANN used for unsupervised learning and dimensionality reduction. It is highly used in various domains, including text, voice, and image data analysis. It can capture the essential characteristics of the data and reduce the input features without losing the information. It is based on transforming the input data into a new compressed dataset by the encoder. Then, the decoder reconstructs the original data from the compressed data. By doing so, the noises or any redundant information can be discarded from the dataset. Compared to the PCA, the autoencoder algorithm is used when the correlation between the dataset variables is nonlinear using a nonlinear activation function such as: (Tanh, sigmoid). Figure 8 illustrates the structure of the autoencoder algorithm. The bottleneck or the code layer will have 20 neurons, the same number as the PCA's selected principal components, to compare the performance of the ANN using both methods.

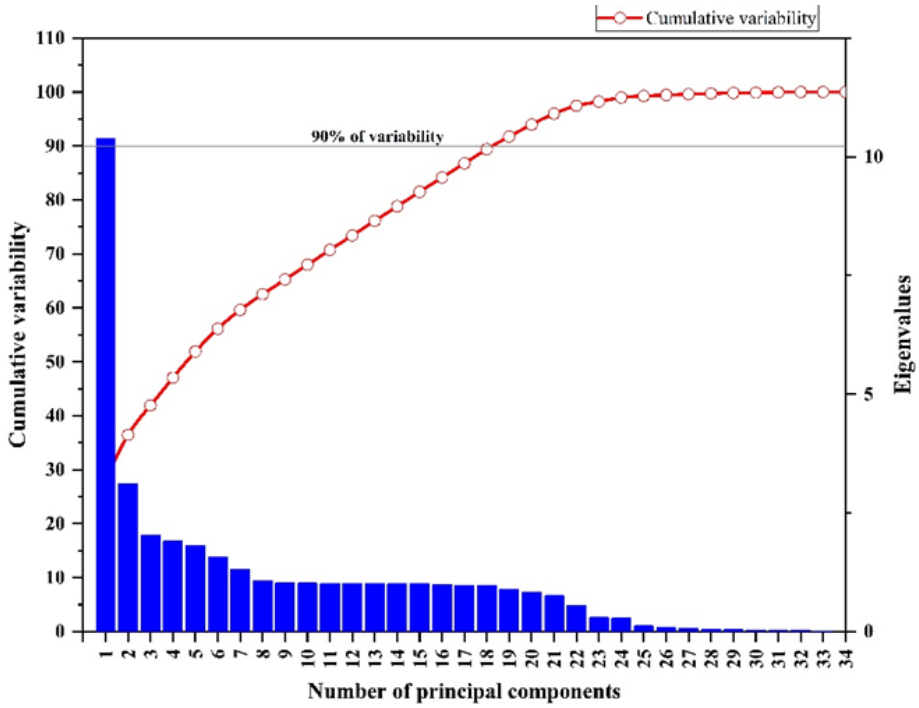

Fig. 7. Eigenvalues and the cumulative variability of the dataset

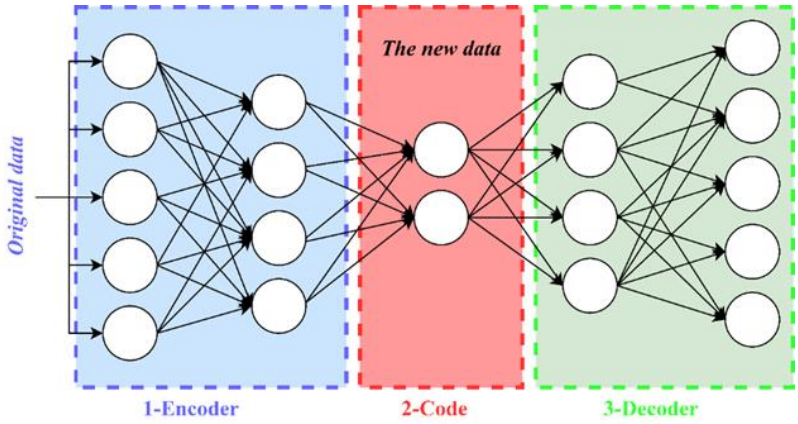

Fig. 8. The autoencoder structure

2.5. Artificial Neural Networks (ANN)

The ANN is supervised machine learning based on training the model on a dataset containing inputs and outputs and testing its performance in predicting unseen cases. It is composed of an input layer, hidden layers, and output layers. The input layer will contain the earthquake and the building characteristics or the transformed input features using the PCA or the autoencoder. A backpropagation (BP) algorithm will train the ANN model. The hidden layers (HL) contain intermediate neurons, and the number of hidden layers and number of neurons (NN) should be optimized to avoid the underfitting or overfitting of the ANN model. The output layer contains three neurons representing the seismic responses (MBS, MIDR, and MRDR). An "Adam" algorithm is used as an optimization algorithm, and "ReLu and Linear" activation functions are used for the hidden and output layers, respectively. The hyperparameters (HL/ NN) are selected by performing the ANN several times, changing them randomly, and selecting the best combination that corresponds to the highest correlation coefficient (R^2) and the lowest mean squared error (MSE). Figure 9 illustrates the ANN structures and the used activation functions.

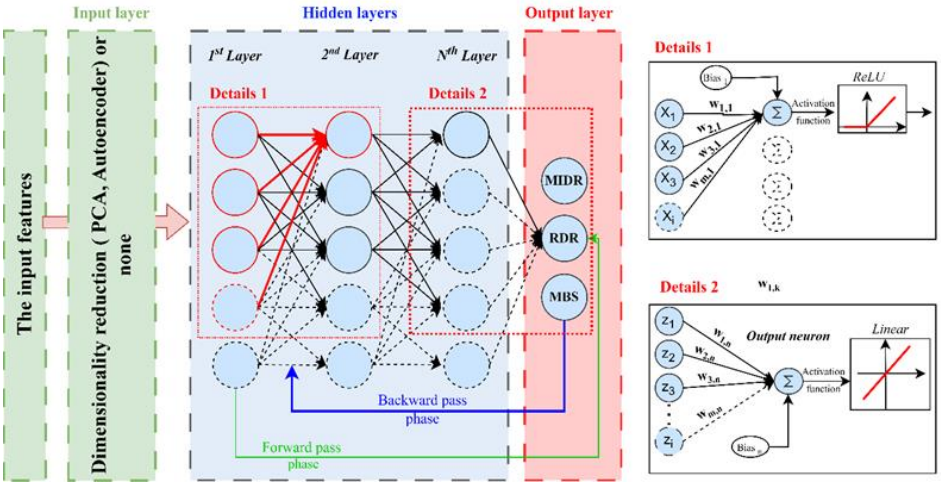

Fig. 9. the structure of the ANN

2.6. Performance of the ANNs

In order to find the best model that can predict the seismic responses accurately, three ANN models have been performed (ANN, PCA-ANN, and Autoencoder-ANN). The dataset is split into training (80%), testing (10%), and validation data (10%). The performance of the ANN will be evaluated using the correlation coefficient (R^2), mean squared error (MSE), and root mean squared error (RMSE), as they are shown in Table 3, where:

$y_{ANN,i}$: is the predicted seismic response.

$y_{NLTHA,i}$: is the calculated seismic response.

$\overline{y_{ANN,i}}$: is the mean value of the predicted seismic response.

$\overline{y_{NLTHA,i}}$: is the mean value of the calculated seismic response.

Table 3. the formulas of the performance coefficients

Performance coefficient	Formula
R^2	$=\frac{\sum(y_{ANN,i}-\overline{y_{ANN,i}})(y_{NLTHA,i}-\overline{y_{NLTHA,i}})}{\sqrt{\sum(y_{ANN,i}-\overline{y_{ANN,i}})^2(y_{NLTHA,i}-\overline{y_{NLTHA,i}})^2}}$
MSE	$=\frac{1}{N}\sum(y_{ANN,i}-y_{NLTHA,i})$
RMSE	$=\sqrt{\frac{1}{N}\sum(y_{ANN,i}-y_{NLTHA,i})}$

Firstly, the ANN model is trained on the generated dataset directly without using any unsupervised techniques (PCA or Autoencoder). It aims to compare the results of using the ANN model with hybrid ANN models regarding predictability. Secondly, a hybrid PCA-ANN model is performed using a dimensionality reduction and twenty principal components (reducing the dimensions from 37 to 20). Finally, another hybrid Autoencoder-ANN model is trained where a coder layer holds 20 neurons (20 dimensions). All the models' hyperparameters have been optimized using random selection and choosing the best combinations. Table 4 summarizes the hyperparameters used in these three models. Table 5 illustrates the performance of the ANN models, where the results represent the mean values of training, testing, and validating.

Table 4. The hyperparameters of the three ANN models

ANN model	Number of neurons	Number hidden layers	Learning rate	Activation function
ANN	60	4	0.01	Relu & linear
PCA-ANN	30	3	0.01	Relu & linear
Autoencoder-ANN	35	2	0.01	Relu & linear

Table 5. The performance of the ANN, PCA-ANN, and Autoencoder-ANN

	MBS			MIDR			MRDR		
	ANN	Auto-ANN	PCA-ANN	ANN	Auto-ANN	PCA-ANN	ANN	Auto-ANN	PCA-ANN
R^2	0.972	0.985	0.986	0.976	0.989	0.9913	0.9745	0.984	0.988
MSE	0.0018	7.6E-05	0.013	0.0017	0.00013	0.0087	0.0051	0.00011	0.0117
RMSE	0.042	0.0086	0.111	0.042	0.0113	0.090	0.071	0.0106	0.1045

Overfitting is a common problem that may occur during the training of ANN model. This can be caused due to the bad selection of hyperparameters such as the number of neurons or number of hidden layers. The overfitting is captured when the performance of the validation data diverges from the training performance as shown in Figure 10. It is represented in a high performance of the training process and low performance of validation data. In Figure 11 depicts the evolution of loss function (MSE) in function of number of epochs for the three ML models.

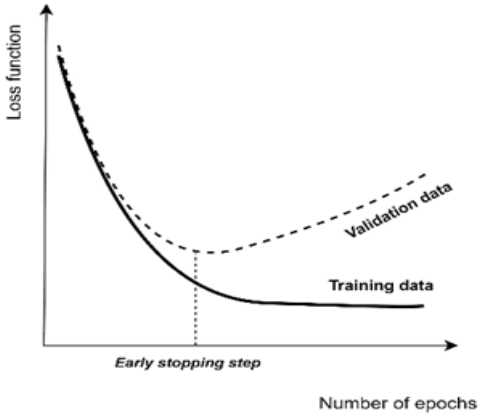

Fig.10 Overfitting in ML models illustration

2.7. Performance of the ANN-Models to Unseen GMs

This section aims to test the performance of the ANNs when the buildings are subjected to 30 unseen GMs. These AGMs matched the identical target response spectra, as shown in Figure 12. Three buildings will be used as a case study (low-, mid-, and high-rise) to check the predictability of the ANN models to unseen cases. IDA curves will be generated and compared to the predicted ones. The 3D fragility surfaces will be constructed using the IDA curves of the MISDR and the MRDR, and then a comparison between these surfaces will be made. The characteristics of the case study buildings are shown in Table 6.

Table 6. The geometric and material characteristics of the case study buildings (low-, mid-, and high-rise)

Parameter	Low-rise	mid-rise	High-rise	Parameter	Low-rise	mid-rise	High-rise
Ns	3	6	9	h1 (m)	0.4	0.45	0.45
Hs (m)	3	3	3	b1 (m)	0.3	0.3	0.35
Nbx	4	4	4	As_col (cm^2)	30.39	30.39	49.23
Lbx (m)	3.2	3.2	3.2	As_beam (cm^2)	25.12	25.12	36.17
Nby	3	3	3	fc28 (MPa)	35	35	35
Lby (m)	3.2	3.2	3.2	fy (GPa)	500	500	500
h (m)	0.4	0.45	0.65	G (kN/m^2)	3	3	3
b (m)	0.4	0.45	0.65	Q (kN/m^2)	1	1	1

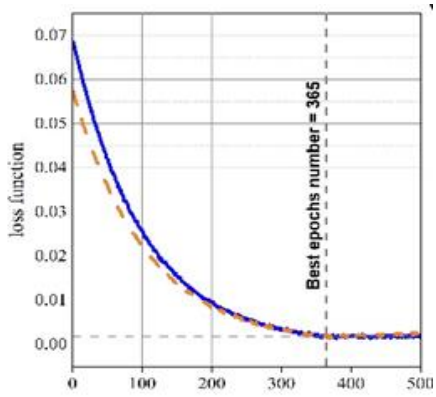
loss function
Best epochs number = 365

(a)

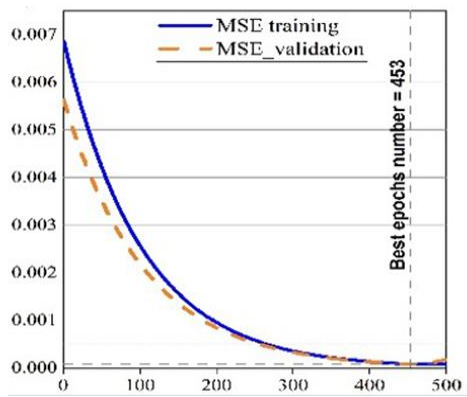
MSE training
MSE_validation
Best epochs number = 453

(b)

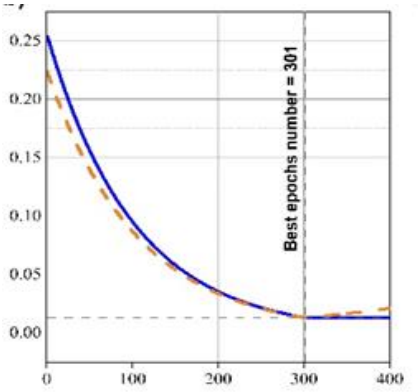
Best epochs number = 301

(c)

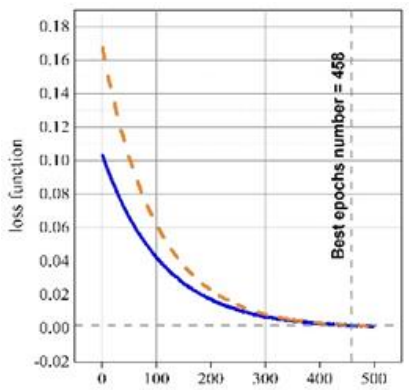
loss function
Best epochs number = 458

(d)

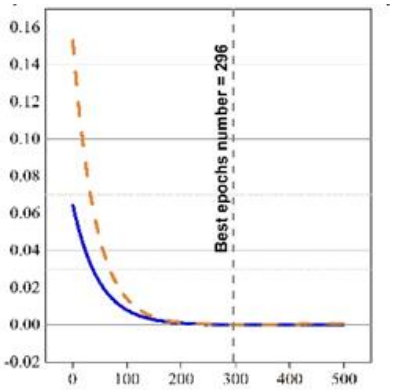
Best epochs number = 296

(e)

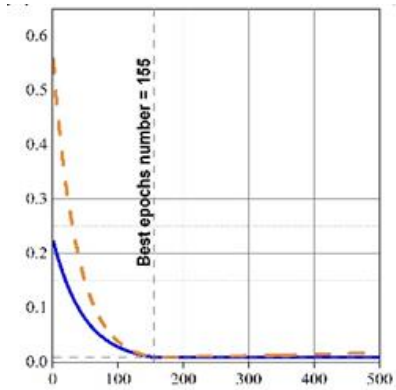
Best epochs number = 155

(f)

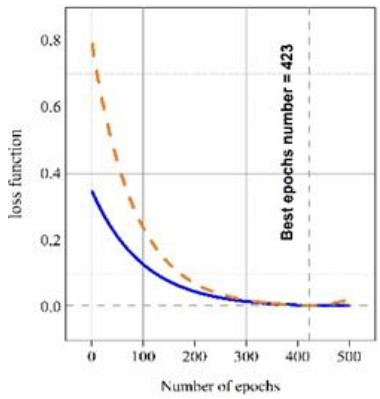

(g)

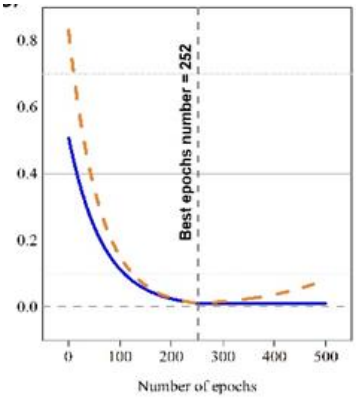

(h)

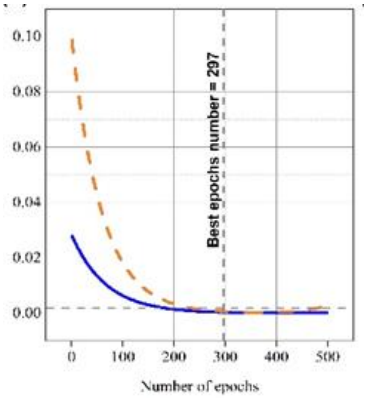

(i)

Fig. 11. Loss function in terms of number of epochs and the best performance position: a) ANN model for predicting the MBS, b) Auto-ANN model for predicting the MBS, c) PCA-ANN model for predicting the MBS, d) ANN model for predicting the MRDR, e) Auto-ANN model for predicting the MRDR, f) PCA-ANN model for predicting the MRDR, g) ANN model for predicting the MIDR, h) Auto-ANN model for predicting the MIDR, i) PCA-ANN model for predicting the MIDR

3. Results

The goal of this paper is not only to predict the seismic response but to generalize the prediction of the outputs based on the training dataset only. In the case study, three buildings were selected to perform the IDA, construct the fragility surfaces, and test the ANN models to predict seismic responses under unseen GMs. Figure 13, Figure 14, and Figure 15 illustrate the IDA points of the three buildings using the NL-THA and the ANN models. The performance criteria of the prediction of the MBS, MIDR and MRDR of the ANN model, PCA-ANN model and Autoencoder-ANN model is summarized in Table 7-8-9.

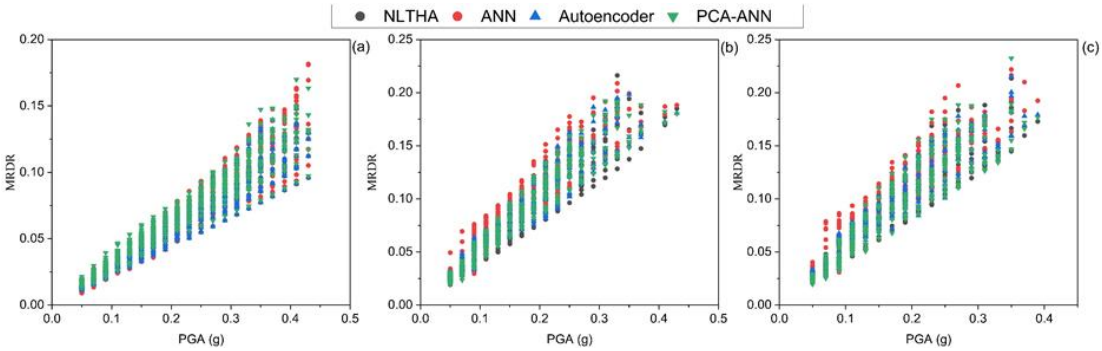

Fig. 13 the MRDR for the three models: a) low-rise, b) mid-rise and c) high-rise

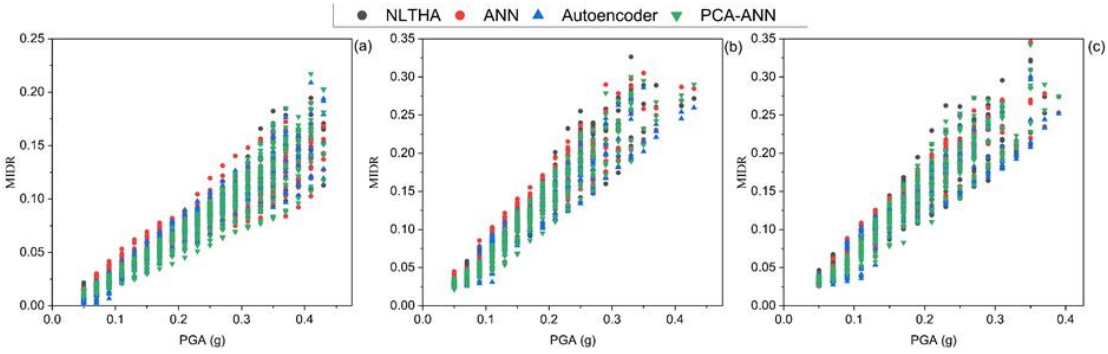

Fig. 14.The MIDR prediction for the three models: a) low-rise, b) mid-rise and c) high-rise

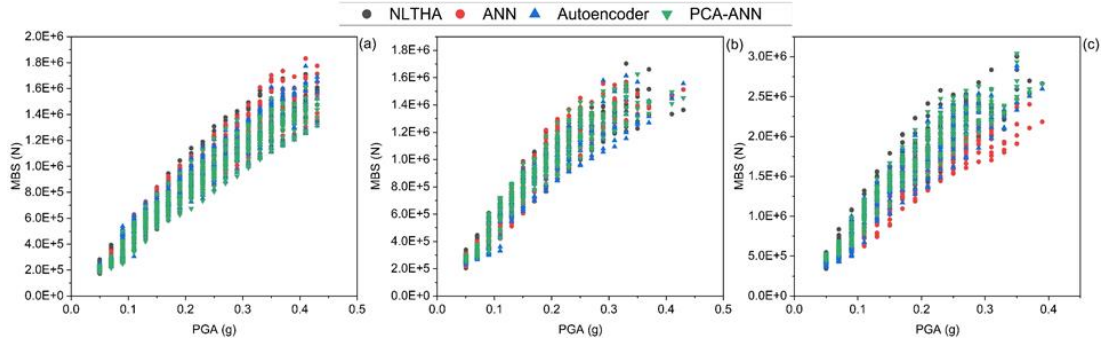

Fig. 15. the MBS prediction for the three models: a) low-rise, b) mid-rise and c) high-rise

Figure 16, Figure 17, Figure 18, Figure 19, Figure 20 and Figure 21 represent the 3D fragility surfaces constructed using the NL-THA and the ANN models for low-, mid-, and high-rise buildings. The accuracy of the prediction of these 3D fragility surfaces is calculated using the same performance criteria (R^2, MSE, and RMSE), and they are summarized in Table 10 and Table 11 for MIDR and MRDR.

Table 7. The performance of the ANN to predict the MBS to unseen GMs.

	MBS								
	Low-rise			Mid-rise			High-rise		
	ANN	Auto-ANN	PCA-ANN	ANN	Auto-ANN	PCA-ANN	ANN	Auto-ANN	PCA-ANN
R^2	0.850	0.964	0.964	0.931	0.965	0.931	0.822	0.964	0.954
MSE	0.025	0.002	0.017	0.016	0.005	0.009	0.084	0.017	0.034
RMSE	0.158	0.051	0.133	0.127	0.072	0.097	0.291	0.133	0.185

Table 8. The performance of the ANN to predict the MIDR to unseen GMs.

	MIDR								
	Low-rise			Mid-rise			High-rise		
	ANN	Auto-ANN	PCA-ANN	ANN	Auto-ANN	PCA-ANN	ANN	Auto-ANN	PCA-ANN
R^2	0.91	0.94	0.93	0.93	0.959	0.958	0.938	0.9550	0.94
MSE	0.0006	9.6E-05	1.0E-04	3.0E-04	8.7E-04	1.90E-04	1.22E-03	1.89E-04	2.48E-04
RMSE	0.025	0.0098	0.0103	0.0174	0.0296	0.0137	0.0348	0.0137	0.0157

Table 9. The performance of the ANN to predict the MRDR to unseen GMs.

	MRDR								
	Low-rise			Mid-rise			High-rise		
	ANN	Auto-ANN	PCA-ANN	ANN	Auto-ANN	PCA-ANN	ANN	Auto-ANN	PCA-ANN
R^2	0.708	0.90	0.909	0.861	0.961	0.962	0.878	0.968	0.9549
MSE	0.0003	0.0001	0.00096	0.0002	7.18E-05	7.07E-04	2.20E-04	5.84E-04	8.16E-05
RMSE	0.0174	0.0101	0.0311	0.0160	0.0084	0.0265	0.0148	0.0241	0.0090

Table 10. The accuracy of the 3D fragility surfaces prediction (MIDR).

	MIDR								
	Low-rise			Mid-rise			High-rise		
	ANN	Auto-ANN	PCA-ANN	ANN	Auto-ANN	PCA-ANN	ANN	Auto-ANN	PCA-ANN
R^2	0.6014	0.9512	0.9139	0.833	0.9917	0.9830	0.971	0.9719	0.9716
MSE	0.0808	0.0007	0.0098	0.059	0.0018	0.0035	0.006	0.0061	0.0062
RMSE	0.2842	0.0258	0.0989	0.244	0.0425	0.0595	0.078	0.0778	0.0784

Table 3. The accuracy of the 3D fragility surfaces prediction (MRDR).

	MRDR								
	Low-rise			Mid-rise			High-rise		
	ANN	Auto-ANN	PCA-ANN	ANN	Auto-ANN	PCA-ANN	ANN	Auto-ANN	PCA-ANN
R^2	0.8361	0.9713	0.9422	0.8993	0.9908	0.9414	0.9052	0.9937	0.9316
MSE	0.0583	0.0062	0.0126	0.0216	0.0020	0.0127	0.0202	0.0013	0.0149
RMSE	0.2416	0.0785	0.1122	0.1471	0.0449	0.1127	0.1420	0.0367	0.1222

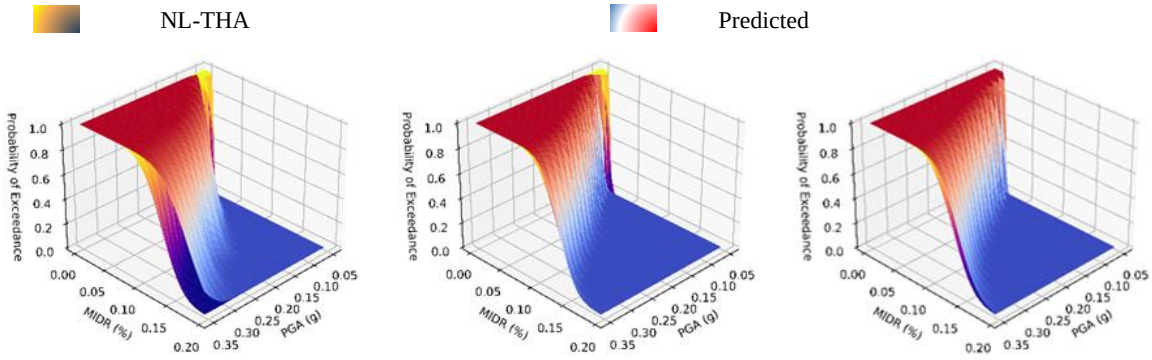

(a) (b) (c)

Fig. 16. 3D Fragility surfaces (NL-THA and ANNs) of the MIDR for low-rise building: a) ANN, b) Autoencoder-ANN and c) PCA-ANN

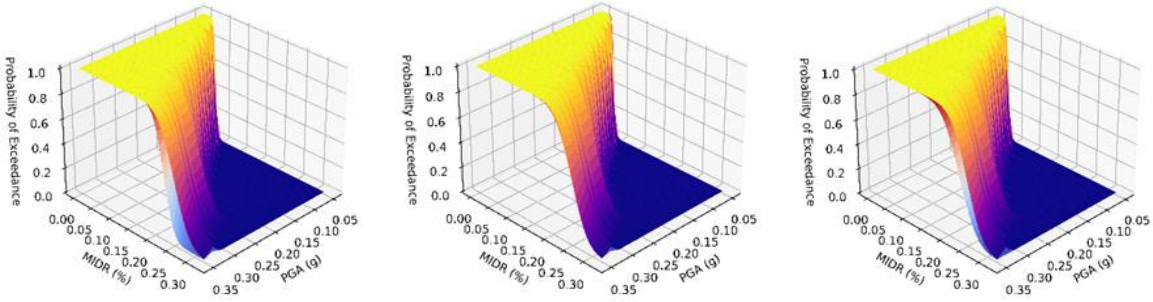

(a) (b) (c)

Fig. 17. 3D Fragility surfaces (NL-THA and ANNs) of the MIDR for mid-rise building: a) ANN, b) Autoencoder-ANN and c) PCA-ANN

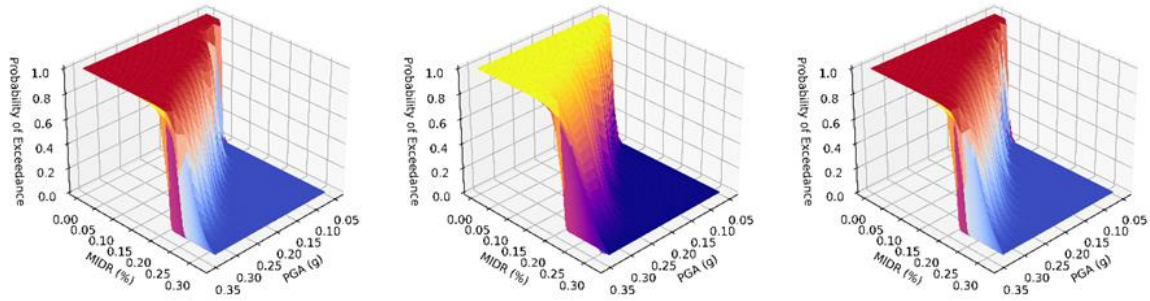

(a) (b) (c)

Fig. 18. 3D Fragility surfaces (NL-THA and ANNs) of the MIDR for high-rise building: a) ANN, b) Autoencoder-ANN and c) PCA-ANN

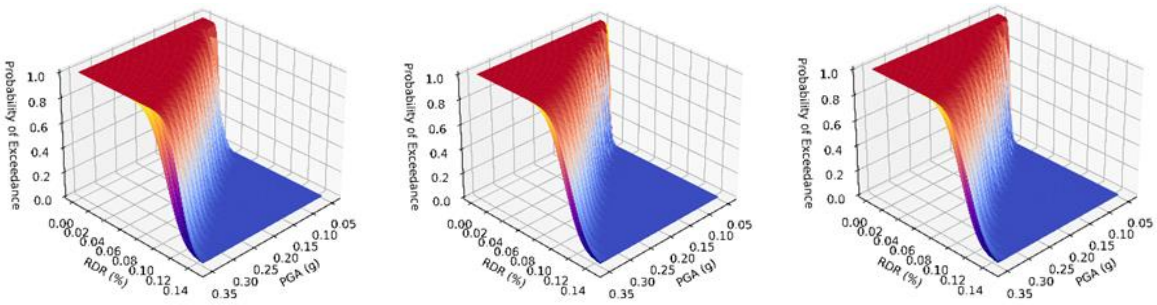

(a) (b) (c)

Fig.19. 3D Fragility surfaces (NL-THA and ANNs) of the MRDR for low-rise building: a) ANN, b) Autoencoder-ANN and c) PCA-ANN

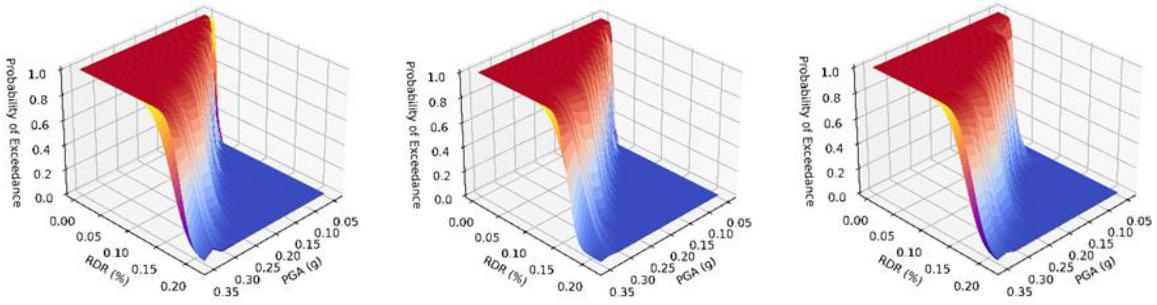

(a) (b) (c)

Fig. 20. 3D Fragility surfaces (NL-THA and ANNs) of the MRDR for mid-rise building: a) ANN, b) Autoencoder-ANN and c) PCA-ANN

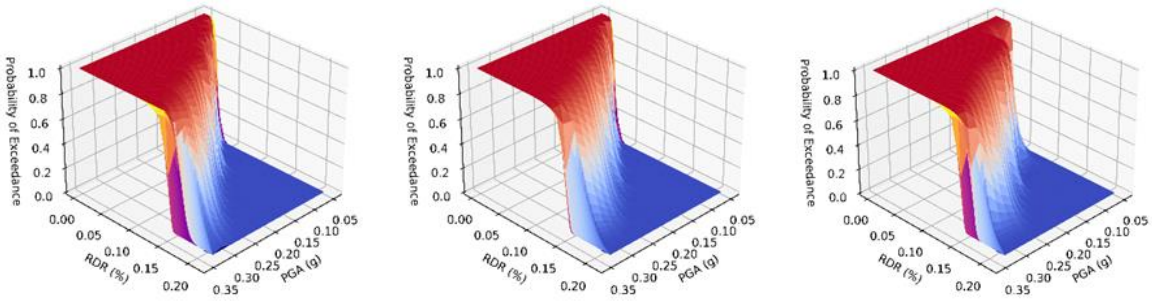

(a) (b) (c)

Fig. 21. 3D Fragility surfaces (NL-THA and ANNs) of the MRDR for mid-rise building: a) ANN, b) Autoencoder-ANN and c) PCA-ANN

4.Discussion

The seismic response is essential for the vulnerability and fragility assessment of new and existing buildings. The NL-THA is considered the most reliable and accurate method to achieve an exact investigation. However, this method is not always suitable due to its complexity and time-consuming. Therefore, many works have been proposed to facilitate the assessment process using techniques like machine learning algorithms. In this paper,

an ANN model has been developed to predict the seismic responses (MBS, MIDR, and MRDR) of RC frame buildings using only the building geometry and earthquake characteristics. It aims to offer analysts a rapid and fast alternative to predict the building's performance and calculate the probability of exceeding a certain damage level.

The paper starts by generating a dataset with more than 190,000 NL-THA performed, and three ANN models were trained (ANN, Autoencoder-ANN, PCA-ANN). Table 5 illustrates that three ANN models achieved a good performance level with correlation coefficients exceeding 97%. The Autoencoder-ANN model showed the lowest MSE and RMSE (0.00007,0.000131 and 0.00011) for MBS, MIDR, and MRDR, respectively. For the PCA-ANN model showed the highest correlation coefficients (98%, 99%, and 98%) during the training process, and the MSE is higher than the ANN's (0.0013,0.0087 and 0.011761) for MBS, MIDR, and MRDR. The hybrid models (PCA and Autoencoder) performed better in training, testing, and validation than the ANNs. Only twenty dimensions have been used to train the ANN. In addition, the dimensionality reduction allowed us to reduce and optimize the ANN model's hyperparameters, as shown in Table 4, which made the training process faster and less complex. This improvement is caused to the ability of the unsupervised techniques to capture the principal components (in the case of the PCA) or the essential features of the dataset (in the case of the Autoencoder). The proposed model was tested on unseen GMs since the work aims to develop an accurate, fast, and generalized method that can be used as an alternative to the NL-THA. Three buildings with different heights were used as a case study, and thirty artificial GMs matched to the same target response spectrum were used to perform the analysis.

Figure 13, Figure 14, and Figure 15 illustrate the IDA points of the (MBS, MIDR, and MRDR) versus the incremented seismic intensity (PGA). Table 7, Table 8, and Table 9 summarized the performance of the prediction. The results showed that the Autoencoder-ANN model has the highest rate of predictability regarding R^2 and MSE. The PCA-ANN model also showed high accuracy in terms of R^2 and MSE and slightly less than the Autoencoder's accuracy. The ANN model showed good predictability but remarkably less than the previous hybrid models for all the ANN models and all three buildings. It can be concluded that using these unsupervised techniques enhanced the accuracy of the prediction, even for unseen GMs.

The 3D fragility surfaces were constructed using the IDA results and compared to the NL-THA fragility surfaces. Figure 16, Figure 17, and Figure 18 illustrate the 3D fragility surfaces of the MIDR using the ANN, Autoencoder-ANN, and PCA-ANN for low-, mid-, and high-rise buildings. Figure 19, Figure 20, and Figure 21 illustrate the 3D fragility surfaces of the MRDR using the ANN, Autoencoder-ANN, and PCA-ANN for low-, mid-, and high-rise buildings. The accuracy of these surfaces to the exact surfaces is summarized in Table 10 and Table 11 for the MIDR and MRDR, respectively. According to these Figures and the tables, it can be noticed that the Autoencoder and the PCA models accurately predict the fragility of surfaces with an R^2> 95% where the Autoencoder models represented the highest correlation coefficient of 95%, 99%,97% for the MIDR and 97%, 99%, and 99% for the MRDR, and the lowest MSE 0.0007,0.0018 and 0.0061 for the MIDR and 0.0062, 0.002 and 0.0013 for the MRDR. The PCA-ANN model also showed high accuracy and slightly less than the Autoencoder-ANN model, with an R^2 of 91%,98%, and 97% for the MIDR and 94%, 94%, and 93% for the MRDR. For the ANN models, they showed an acceptable correlation with an R^2 of 83%, 89%, and 90% for the MRDR and 60%, 83%, and 97% for the MIDR and an MSE of 0.08, 0.05, and 0.0062 for the MIDR and 0.5, 0.02 and 0.02 for the MRDR.

Given these results, the Autoencoder-ANN is the most suitable hybrid method to predict seismic responses. Its accuracy is not limited to seen GMs but to unseen ones. Also, the

PCA-ANN model presented an excellent model, slightly less accurate than the Autoencoder regarding the predictability of the IDA points and fragility surfaces. The use of the hybrid models improved the accuracy and optimized the ANN's hyperparameters, making the ANN model more generalized to unseen scenarios.

5.Conclusion

The paper presents a new approach for predicting seismic responses with high speed and accuracy. The approach utilizes unsupervised algorithms and Artificial Neural Networks (ANN) to predict critical seismic parameters such as MBS, MIDR and MRDR. This new approach can be helpful in the field of earthquake engineering and research, as it can provide better understanding of the seismic behavior of structures.

The paper compares the performance of three different ML models. The first model is an ANN without any modification to the input features. The second model is a combination of an autoencoder and an ANN, where autoencoder algorithm is used to obtain the input features for ANN. The third model is a combination of Principal Component Analysis (PCA) and ANN, where PCA is used to reorient and reduce the input data. These ML models are compared with the NLTHA results in terms of R^2, MSE and RMSE.

The comparative study provides several insights into the performance of different models:

- The ML-based approach presented a quick alternative to the NLTHA, where it can be used as an alternative by the engineers to fast assess the seismic response of RC frame buildings without the need for modeling to processing time.
- The use of hybrid approaches as PCA-ANN and Autoencoder-ANN made the prediction more accurate and enhanced the performance and outputs results and reduced the MSE.
- The ML models were able to reach a high accuracy by using only the geometry characteristics which mean that the engineer can use it on the field without the need to any calculations or FEM software.
- The Autoencoder made the ANN training more accurate, and it reduced the MSE remarkably compared to PCA-ANN and ANN models.
- The use of hybrid models made the ANN training much faster and less complex due to the dimensionality reduction and data reorientation and make the ANN train on the principal components.
- The hybrid model reduces the hyperparameter numbers such as number of neurons and number of hidden layers due to the input features reduction.
- The ML-based can be a useful tool for vulnerability and fragility assessments due to it high accuracy and reduce computational time and its simplicity.

The hybrid model is a useful tool for quickly investigating the seismic vulnerability and fragility of structures. However, it should be noted that the accuracy of the model's predictions is limited to reinforced concrete frame structures with specific geometry characteristics mentioned in the paper. To ensure accurate results, it is recommended not to use parameters that exceed the upper bound of the training dataset. Doing so may affect the accuracy of the model's predictions.

Appendix A

Table A1. The eighty artificial ground motions and their characteristics used to generate the dataset.

GMs	PGA (g)	PGV (cm/sec)	PGD (cm)	AI	Ic	CAV (cm/sec)	VSI (cm)	HI (cm)	A95 (g)	PP (sec)	SD (sec)
GM 1	0.16	14.11	20.11	0.52	0.04	567.24	59.85	55.06	0.15	0.40	12.78
GM 2	0.19	14.32	9.15	0.51	0.04	545.23	61.57	57.10	0.19	0.20	11.38
GM 3	0.19	14.66	13.81	0.50	0.04	543.61	63.62	58.87	0.18	0.18	12.02
GM 4	0.22	18.64	15.45	0.52	0.04	554.85	61.65	56.96	0.22	0.26	11.88
GM 5	0.21	15.38	31.25	0.47	0.04	531.61	61.30	54.65	0.21	0.38	11.99
GM 6	0.18	13.76	8.97	0.53	0.04	561.33	63.73	57.84	0.17	0.22	11.86
GM 7	0.23	13.48	10.61	0.46	0.04	525.61	64.23	59.44	0.23	0.20	11.65
GM 8	0.21	16.43	18.57	0.50	0.04	543.66	61.33	56.10	0.21	0.18	12.40
GM 9	0.17	13.75	14.87	0.43	0.03	501.45	59.01	54.77	0.17	0.40	10.55
GM 10	0.18	13.25	7.55	0.35	0.03	439.99	63.80	57.74	0.18	0.36	9.65
GM 11	0.15	14.28	7.21	0.41	0.03	490.52	60.75	55.85	0.15	0.22	10.96
GM 12	0.19	13.93	6.34	0.50	0.04	546.92	62.42	58.53	0.19	0.26	12.25
GM 13	0.17	14.99	7.42	0.55	0.04	560.44	64.80	60.13	0.17	0.16	10.45
GM 14	0.19	12.39	4.40	0.41	0.03	468.87	64.58	58.89	0.18	0.26	10.14
GM 15	0.17	15.18	8.90	0.33	0.03	418.10	59.98	55.27	0.17	0.16	9.40
GM 16	0.18	16.73	12.04	0.39	0.03	472.72	61.43	56.29	0.17	0.20	10.20
GM 17	0.21	15.10	6.76	0.34	0.03	422.32	61.96	56.02	0.20	0.32	9.08
GM 18	0.16	12.79	9.33	0.50	0.04	587.56	59.82	55.51	0.15	0.40	14.25
GM 19	0.19	16.89	20.74	0.47	0.03	558.46	65.73	59.56	0.19	0.36	13.36
GM 20	0.16	13.91	9.36	0.49	0.04	588.11	61.13	56.49	0.16	0.22	15.16
GM 21	0.16	14.25	5.40	0.57	0.04	628.21	62.70	58.45	0.15	0.16	14.80
GM 22	0.18	13.23	8.54	0.51	0.04	579.00	64.44	59.07	0.18	0.26	13.76
GM 23	0.20	14.88	13.59	0.58	0.04	588.32	64.21	59.57	0.19	0.18	12.84
GM 24	0.17	12.02	8.39	0.40	0.03	515.35	59.72	56.04	0.17	0.16	14.70
GM 25	0.17	17.88	11.52	0.49	0.04	579.15	61.86	57.78	0.16	0.20	13.85
GM 26	0.19	14.01	12.36	0.39	0.03	508.24	57.89	54.05	0.19	0.32	14.31
GM 27	0.15	22.68	53.92	0.43	0.03	494.46	58.71	55.17	0.14	0.28	10.62
GM 28	0.15	15.24	4.38	0.40	0.03	468.88	61.65	57.47	0.15	0.34	10.34
GM 29	0.18	24.89	32.01	0.46	0.04	524.63	62.76	57.31	0.17	0.30	16.74
GM 30	0.24	16.87	7.59	0.44	0.03	492.32	61.89	57.19	0.24	0.16	10.35
GM 31	0.18	11.58	7.91	0.40	0.03	453.14	64.66	58.25	0.17	0.38	10.04
GM 32	0.18	29.46	41.92	0.37	0.03	443.87	57.01	55.76	0.17	0.22	9.66

GM 33	0.20	20.19	24.56	0.41	0.03	477.89	61.34	58.43	0.20	0.38	10.57
GM 34	0.24	15.01	6.42	0.51	0.04	561.26	60.64	56.34	0.24	0.16	12.83
GM 35	0.19	16.13	10.13	0.32	0.03	408.98	58.44	54.50	0.19	0.18	10.54
GM 36	0.16	12.97	6.89	0.40	0.03	564.23	61.60	53.14	0.16	0.36	14.24
GM 37	0.17	104.02	300.93	0.63	0.04	785.25	48.45	52.69	0.17	0.30	16.41
GM 38	0.18	12.77	9.02	0.43	0.03	586.99	56.76	51.90	0.17	0.24	13.71
GM 39	0.17	12.85	11.58	0.46	0.03	612.88	58.90	52.80	0.16	0.30	14.16
GM 40	0.15	33.28	90.36	0.44	0.03	593.89	58.27	53.39	0.15	0.32	14.39
GM 41	0.13	11.18	7.23	0.41	0.03	588.53	54.63	52.33	0.13	0.40	13.90
GM 42	0.15	38.52	124.98	0.47	0.03	680.39	56.90	53.23	0.15	0.36	20.67
GM 43	0.17	15.18	19.05	0.44	0.03	623.98	57.08	54.43	0.16	0.30	15.23
GM 44	0.13	30.39	130.65	0.59	0.03	905.73	57.45	53.37	0.13	0.28	24.96
GM 45	0.18	30.64	121.62	0.50	0.04	545.28	61.88	56.41	0.18	0.38	12.40
GM 46	0.15	13.73	26.47	0.60	0.03	906.12	57.12	53.26	0.14	0.32	24.16
GM 47	0.16	37.30	210.98	0.67	0.04	996.46	58.37	54.64	0.15	0.28	25.90
GM 48	0.15	16.38	10.19	0.70	0.04	983.07	60.61	54.21	0.15	0.24	23.87
GM 49	0.14	10.51	13.95	0.65	0.04	963.25	58.47	53.19	0.14	0.28	25.55
GM 50	0.14	41.64	159.92	0.67	0.04	1037.31	54.92	53.06	0.14	0.18	30.23
GM 51	0.15	13.97	21.95	0.63	0.03	943.91	57.09	52.38	0.15	0.26	25.03
GM 52	0.15	31.67	201.03	0.65	0.04	967.57	55.53	53.23	0.14	0.16	25.46
GM 53	0.14	16.77	29.56	0.70	0.04	991.50	62.04	56.74	0.13	0.24	25.21
GM 54	0.15	21.46	114.56	0.66	0.04	950.93	62.88	59.05	0.15	0.24	24.22
GM 55	0.16	15.49	79.16	0.69	0.04	977.16	61.59	56.89	0.16	0.28	23.85
GM 56	0.19	12.23	7.14	0.45	0.04	510.95	62.72	57.80	0.18	0.22	12.88
GM 57	0.14	19.87	106.57	0.68	0.04	981.23	60.71	54.27	0.14	0.24	24.55
GM 58	0.14	23.68	129.52	0.69	0.04	1006.77	60.98	56.66	0.14	0.26	26.05
GM 59	0.14	22.31	147.84	0.68	0.04	1025.23	56.65	52.42	0.14	0.40	28.88
GM 60	0.17	28.67	186.34	0.69	0.04	989.14	59.66	56.10	0.16	0.32	25.36
GM 61	0.14	14.10	40.27	0.70	0.04	991.06	60.10	55.87	0.14	0.16	24.87
GM 62	0.17	16.89	44.37	0.43	0.03	592.90	63.35	54.69	0.17	0.36	14.49
GM 63	0.16	12.64	3.39	0.52	0.03	660.31	61.54	55.08	0.16	0.36	14.55
GM 64	0.18	14.31	18.33	0.47	0.03	617.75	60.10	54.91	0.17	0.28	13.93
GM 65	0.17	11.51	15.65	0.47	0.03	624.10	60.11	53.38	0.16	0.28	14.42
GM 66	0.16	12.85	10.56	0.46	0.03	607.56	60.32	54.61	0.15	0.20	14.17
GM 67	0.22	24.04	38.87	0.48	0.04	541.49	63.77	59.20	0.21	0.20	12.39
GM 68	0.14	12.78	10.24	0.46	0.03	630.85	57.82	54.31	0.13	0.40	14.72
GM 69	0.16	22.10	58.72	0.45	0.03	595.52	63.40	57.76	0.15	0.32	13.75

GM 70	0.19	158.68	1376.71	0.67	0.04	876.57	52.93	55.44	0.19	0.30	25.31
GM 71	0.16	13.53	6.32	0.40	0.03	560.41	61.40	52.97	0.16	0.46	14.14
GM 72	0.16	38.57	116.48	0.52	0.03	676.30	58.32	54.42	0.15	0.30	15.47
GM 73	0.19	13.18	8.14	0.46	0.03	606.51	57.80	52.84	0.18	0.24	13.71
GM 74	0.17	12.60	10.78	0.46	0.03	614.91	58.90	52.79	0.17	0.30	14.16
GM 75	0.15	11.51	17.89	0.48	0.03	640.40	59.84	54.59	0.15	0.32	15.12
GM 76	0.14	12.42	8.64	0.46	0.03	620.74	56.73	54.02	0.13	0.40	14.24
GM 77	0.16	13.93	14.37	0.42	0.03	564.42	60.17	53.84	0.15	0.36	13.24
GM 78	0.19	15.51	10.81	0.39	0.03	478.98	60.31	55.50	0.18	0.18	13.59
GM 79	0.18	23.61	32.97	0.45	0.03	639.30	55.32	53.26	0.17	0.30	16.54
GM 80	0.19	15.27	13.54	0.50	0.04	542.96	63.50	57.38	0.18	0.24	11.56

References

[1] Benbokhari A, Benazouz C, A M, R M. Seismic vulnerability and fragility assessment of a strategic building in Algeria. Jun. 2023.

[2] Naddaf M. Turkey-Syria earthquake: what scientists know. Nature. 2023 [Epub ahead of print]. doi: 10.1038/d41586-023-00364-y. https://doi.org/10.1038/d41586-023-00364-y

[3] Petak W. Earthquake Resilience through Mitigation: A System Approach. Jan. 2002.

[4] Full article: Review of Seismic Risk Mitigation Policies in Earthquake-Prone Countries: Lessons for Earthquake Resilience in the United States. [Accessed Jul. 07, 2023]. [Online]. Available: https://www.tandfonline.com/doi/full/10.1080/13632469.2021.1911889

[5] Kassem MM, Mohamed Nazri F, Noroozinejad Farsangi E. Development of seismic vulnerability index methodology for reinforced concrete buildings based on nonlinear parametric analyses. MethodsX. Jan. 2019;6:199-211. https://doi.org/10.1016/j.mex.2019.01.006

[6] Li SQ, Chen YS, Liu HB, Del Gaudio C. Empirical seismic vulnerability assessment model of typical urban buildings. Bull Earthquake Eng. Mar. 2023;21(4):2217-2257. https://doi.org/10.1007/s10518-022-01585-8

[7] Aggarwal Y, Saha SK. An improved rapid visual screening method for seismic vulnerability assessment of reinforced concrete buildings in Indian Himalayan region. Bull Earthquake Eng. Jan. 2023;21(1):319-347. https://doi.org/10.1007/s10518-022-01537-2

[8] HAZUS-MH Flood Loss Estimation Methodology. II. Damage and Loss Assessment. Nat Hazards Rev. 2006;7(2):72. https://doi.org/10.1061/(ASCE)1527-6988(2006)7:2(72)

[9] Lantada N et al. Seismic hazard and risk scenarios for Barcelona, Spain, using the Risk-UE vulnerability index method. Bull Earthquake Eng. Apr. 2010;8(2):201-229. https://doi.org/10.1007/s10518-009-9148-z

[10] Kassem MM, Mohamed Nazri F, Noroozinejad Farsangi E. Development of seismic vulnerability index methodology for reinforced concrete buildings based on nonlinear parametric analyses. MethodsX. Jan. 2019;6:199-211. https://doi.org/10.1016/j.mex.2019.01.006

[11] Alilou AAR, Pouraminian M. Seismic Fragility Assessment of RC Frame Equipped by Visco-Elastic Dampers Using NLTHA and FNA. AJEAS. Jul. 2019;12(3):359-367. https://doi.org/10.3844/ajeassp.2019.359.367

[12] Chang SY. Accuracy of Time History Analysis of Impulses. J Struct Eng. Mar. 2003;129(3):357-372. https://doi.org/10.1061/(ASCE)0733-9445(2003)129:3(357)
[13] Progressive Analysis Procedure for Progressive Collapse. J Perform Constr Facil. 2004;18(2):79. https://doi.org/10.1061/(ASCE)0887-3828(2004)18:2(79)
[14] Rahgozar N, Pouraminian M, Rahgozar N. Reliability-based seismic assessment of controlled rocking steel cores. J Build Eng. Dec. 2021;44:102623. https://doi.org/10.1016/j.jobe.2021.102623
[15] A pushover seismic analysis method for asymmetric and tall buildings. J Chin Inst Eng. 2015;38(8). https://doi.org/10.1080/02533839.2015.1056553
[16] Pushover procedure for seismic analysis of buildings. Prog Struct Eng Mater. 1998;1(3-4). https://doi.org/10.1002/pse.2260010317
[17] Rosti A, Rota M, Penna A. An empirical seismic vulnerability model. Bull Earthquake Eng. Jun. 2022;20(8):4147-4173. https://doi.org/10.1007/s10518-022-01374-3
[18] Seismic vulnerability assessment using regional empirical data. Earthquake Eng Struct Dyn. [Accessed Jul. 07, 2023]. [Online]. Available: https://onlinelibrary.wiley.com/doi/abs/10.1002/eqe.572
[19] Asgarkhani N, Kazemi F, Jakubczyk-Gałczyńska A, Mohebi B, Jankowski R. Seismic response and performance prediction of steel buckling-restrained braced frames using machine-learning methods. Eng Appl Artif Intell. Feb. 2024;128:107388. https://doi.org/10.1016/j.engappai.2023.107388
[20] Gholizadeh S, Salajegheh J, Salajegheh E. An intelligent neural system for predicting structural response subject to earthquakes. Advances in Engineering Software. 2009 Aug;40(8):630-9. https://doi.org/10.1016/j.advengsoft.2008.11.008
[21] Buildings, Predicting Dynamic Response of Structures under Earthquake Loads Using Logical Analysis of Data. Accessed: Feb. 24, 2024. https://www.mdpi.com/2075-5309/8/4/61
[22] Vafaei M, bin Adnan A, Abd. Rahman AB. Real-time Seismic Damage Detection of Concrete Shear Walls Using Artificial Neural Networks. Journal of Earthquake Engineering. 2013 Jan;17(1):137-54. https://doi.org/10.1080/13632469.2012.713559
[23] Morfidis K, Kostinakis K. Approaches to the rapid seismic damage prediction of r/c buildings using artificial neural networks. Engineering Structures. 2018 Jun;165:120-41. https://doi.org/10.1016/j.engstruct.2018.03.028
[24] Oh BK, Glisic B, Park SW, Park HS. Neural network-based seismic response prediction model for building structures using artificial earthquakes. Journal of Sound and Vibration. 2020 Mar;468:115109. https://doi.org/10.1016/j.jsv.2019.115109
[25] Won J, Shin J. Machine learning-based approach for seismic damage prediction method of building structures considering soil-structure interaction. Sustainability (Switzerland). 2021;13(8). https://doi.org/10.3390/su13084334
[26] Kalakonas P, Silva V. Seismic vulnerability modelling of building portfolios using artificial neural networks. Earthquake Engineering & Structural Dynamics. 2022;51(2):310-27. https://doi.org/10.1002/eqe.3567
[27] Seo J, Dueñas-Osorio L, Craig JI, Goodno BJ. Metamodel-based regional vulnerability estimate of irregular steel moment-frame structures subjected to earthquake events. Engineering Structures. 2012 Dec;45:585-97. https://doi.org/10.1016/j.engstruct.2012.07.003
[28] Hait P, Sil A, Choudhury S. Seismic damage assessment and prediction using artificial neural network of RC building considering irregularities. Journal of Structural Integrity and Maintenance. 2020 Jan;5(1):51-69. https://doi.org/10.1080/24705314.2019.1692167
[29] Mangalathu S, Heo G, Jeon J-S. Artificial neural network based multi-dimensional fragility development of skewed concrete bridge classes. Engineering Structures. 2018 May;162:166-76. https://doi.org/10.1016/j.engstruct.2018.01.053

[30] Baylon M, Garduque J, Lineses R, Loriaga N. Seismic Vulnerability Assessment of Gilbert Bridge in Laoag, Ilocos Norte Using Capacity -Spectrum Method. 2020.
[31] Rachedi M, Matallah M, Kotronis P. Seismic behavior & risk assessment of an existing bridge considering soil-structure interaction using artificial neural networks. Engineering Structures. 2021 Apr;232:111800. https://doi.org/10.1016/j.engstruct.2020.111800
[32] Belejo A, Barbosa AR, Bento R. Influence of ground motion duration on damage index-based fragility assessment of a plan-asymmetric non-ductile reinforced concrete building. Engineering Structures. 2017 Nov;151:682-703. https://doi.org/10.1016/j.engstruct.2017.08.042
[33] Jalayer F, Ebrahimian H, Miano A, Manfredi G, Sezen H. Analytical fragility assessment using unscaled ground motion records. Earthquake Engineering & Structural Dynamics. 2017;46(15):2639-63. https://doi.org/10.1002/eqe.2922
[34] A probabilistic approach to ground-motion selection for engineering design | Bulletin of the Seismological Society of America | GeoScienceWorld. Accessed: Jul. 07, 2023.
[35] Evaluation of ground motion selection and modification procedures using synthetic ground motions - Kwong - 2015 - Earthquake Engineering & Structural Dynamics - Wiley Online Library. Accessed: Jul. 07, 2023.